VII International Conference on Particle-Based Methods
PARTICLES 2021
P. Wriggers, M. Bischoff, E. Oñate, M. Bischoff, A. Düster & T. Zohdi (Eds)

OPTIMAL DESIGN OF PARTICLE DAMPERS FOR STRUCTURES WITH LOW FIRST EIGENFREQUENCY UNDER FORCED VIBRATION

Niklas Meyer[1], **Robert Seifried**[1]

[1] Institute of Mechanics and Ocean Engineering, Hamburg University of Technology
Eißendorfer Straße 42, 21073 Hamburg, Germany
n.meyer@tuhh.de/robert.seifried@tuhh.de, www.tuhh.de/mum

Key words: Particle damping, Energy dissipation, Frequency response function, Rolling bed

Abstract. Recently, the rolling attribute of spheres has been used to develop efficient particle dampers for horizontal low amplitude vibrations. As long as the particle container's acceleration stays below the gravitational acceleration, this rolling effect of spheres can be used. Hereby, the estimation of the damper's energy dissipation is accurately possible using analytical formulas.
In this paper, the workflow for a systematic damper design for an underlying structure of low first eigenfrequency under forced vibration is presented. The analytical formulas describing the dampers energy dissipation are coupled to a modal reduced model of the utilized vibrating structure. Then an analytical expression for an optimal damper design is derived. Also, the calculation scheme to obtain the frequency response function of the system is presented. As application example, a simple beam-like structure is used, whereby its base point is subjected to a harmonic motion of variable frequency using a linear drive. The particle damper is mounted at the tip of the beam and its velocity is measured using a laser scanning vibrometer. Thus, the frequency response function is obtained experimentally. A good agreement between analytical and experimental obtained frequency response function is achieved for the optimized particle damper, validating the presented approach.

1 Introduction

Forced vibrations are one main reason for structural failure. If a system gets excited near its eigenfrequency large vibration amplitudes might occur, having a huge influence on the system's durability. To reduce such large vibrations amplitudes, passive damping techniques are often used. Classical liquid dampers are mostly seen for these applications. Those dampers are well studied and mathematically easy to describe. However, liquid dampers fail under harsh environmental conditions and do need an anchor point. Thus, for applications where liquid dampers are not suitable, particle dampers are becoming more and more popular.

Hereby, containers are attached to the vibrating structure and filled with granular material. Due to structural vibrations, momentum is transferred to the granular material which interacts with each other. As a result, energy is dissipated by impacts and frictional phenomena between the particles. Particle dampers are cost-efficient devices, add only little mass to the primary system [1], and might be applied to a wide frequency range [2]. Furthermore, they are robust against harsh environmental conditions [3, 4], like in spacecraft applications [5]. Although particle dampers show huge potential, their design is still a challenging task. This is because particle motion, also called motion mode, and energy dissipation correlate in a non-trivial way, which is often poorly understood. Identifying these correlations is still part of ongoing research, see [6–14].
Especially, for systems with low first eigenfrequency, the use of particle dampers is rarely seen. This is because the particle container's acceleration is often below the gravitational acceleration for such systems. In consequence, particles begin to stick and no relative motion between particles and container is obtained and thus only little amount of energy is dissipated [15]. To overcome this problem, the rolling attribute of spheres can be used for horizontal vibrations. Instead of sticking, the particles slide and roll over the container base. For vibration amplitudes below a certain threshold value, no synchronous particle motion is seen. This is called scattered state and results in a comparatively low energy dissipation. However, for vibrations amplitudes above the threshold amplitude, a synchronous motion is obtained. Here, the particles form one particle block and collide inelastically with the container walls resulting in high energy dissipation. This state is called rolling bed motion mode. For both motion modes, analytical equations describing the energy dissipation are derived and are validated by comparison to the energy dissipation of a driven particle container.
In this paper, such a damper design is adopted to damp a structure of low first eigenfrequency under forced vibration. Therefore, the energy dissipation formulas of the motion modes are coupled to a modal reduced model of the later utilized structure. Thus, the frequency response function (FRF) can be obtained. Based on this, a formula for an optimal damper design is derived. For validation, a simple beam-like structure is used. The base point of the beam is subjected to a harmonic motion of variable frequency using a linear drive. The particle damper is mounted at the tip of the beam and its velocity is measured using a laser scanning vibrometer. Thus, the frequency response function is measured and compared to the numerical results based on the analytical formulas.
This paper is organized in the following way: In Sect. 2 the occurring motion modes for low-intensity horizontal vibrations are introduced. In the following Sect. 3 the analytical formulas for the energy dissipation are explained. Then, in Sect. 4 the coupling procedure of the analytical formulas to the modal reduced model of the underlying structure is presented and validated by comparisons to experiments. Finally, in Sect. 5 the conclusion is given.

2 Motion modes

The motion mode describes the motion of a particle bed inside a vibrating container, when the particle container is subjected to a sinusoidally motion of the form $x_\mathrm{c} =$

$X\sin(\Omega t)$, with container amplitude X and angular frequency $\Omega = 2\pi f$. The corresponding container velocity and acceleration follow as $\dot{x}_\mathrm{c} = \dot{X}\cos(\Omega t)$ and $\ddot{x}_\mathrm{c} = -\ddot{X}\sin(\Omega t)$ with $\dot{X} = X\Omega$ and $\ddot{X} = X\Omega^2$. Using such an excitation, different motion modes of the particle bed can be observed, like solid-like, local fluidization, global fluidization, convection, Leidenfrost effect, bouncing bed, or buoyancy convection [16]. Various influence parameters affect the occurring motion mode, like excitation intensity and frequency but also gravity, excitation direction, or particle size [6–14].
For horizontal vibrations of low acceleration amplitude, $\ddot{X} < g$ with g being the gravitational acceleration, two different motion modes can be observed if spherical particles on flat container bases are used. An example of such a container is shown in Fig. 3 in form of the later utilized particle damper. The observed motion modes inside this container are called scattered and rolling bed and are shown in Fig. 1. Both motion modes depend on the optimal stroke X_opt, which is obtained to

$$X_\mathrm{opt} \approx 0.4h, \tag{1}$$

with h being the clearance of the particle bed to the opposite container wall as indicated in Fig. 1. Detailed explanations on the meaning of the optimal stroke X_opt will be given later.
The scattering motion mode occurs for container amplitude $X < X_\mathrm{opt}$. This motion mode is similar to the gaslike state observed by Sack [17] under the condition of weightlessness. The motion mode is characterized by the particles' non-regular movement. Thus, in Fig. 1 just a possible movement of the particles is shown. Particles are hitting each other and the container walls at random phases. A higher vibration amplitude leads to more collisions while a higher clearance leads to fewer collisions.
The second motion mode is called rolling bed. Here, the particle bed moves as one single particle block for $X > X_\mathrm{opt}$. Thus, the translational and rotational velocities of each single particle are assumed to be identical. The particle bed is pushed by the container until the container reaches its maximum velocity, i.e. at $\Omega t = n\pi$ with $n \in \mathbb{N}$. At this time point the container is at $x_\mathrm{c} = 0$ and its velocity is $\dot{x}_\mathrm{c} = \dot{X}$. Due to this pushing, almost no rotational movement of the particles is seen up to this time point, i.e. $\dot{\varphi}_\mathrm{p} = 0$. When the particle container has reached its maximum velocity and decelerates, the particles leave the container wall and start rolling due to friction with the container base. The particle bed collides inelastically with the opposite container wall at the impact time point t_i. During this impact multiple inter-particle and particle–wall contacts occur. Although, by each impact, only a small amount of energy is dissipated, in sum a perfectly inelastic collision of the particle bed with the container wall is achieved [18, 19]. Thus, the velocity of the particle bed after impact is $\dot{x}_\mathrm{p}^+(t_\mathrm{i}) = \dot{x}_\mathrm{c}^+(t_\mathrm{i})$ with $\dot{x}_\mathrm{p}$ being the velocity of each single particle. During this impact, the rotational movement of the particles stops. This procedure is repeated when the particle container moves in the other direction. Hence, in sum two particle impacts with the container walls occur during one vibration cycle.

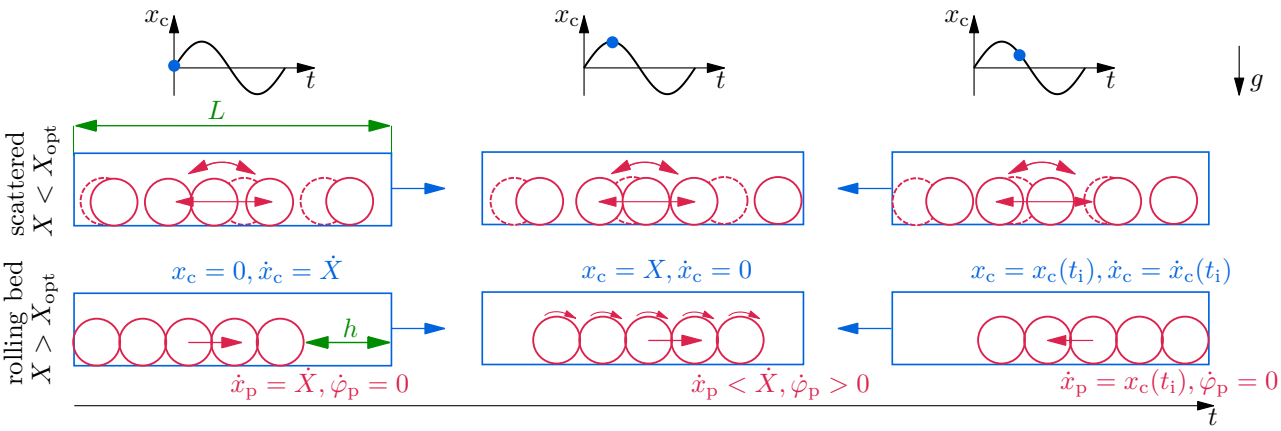

Figure 1: Motion modes at different container strokes for low acceleration amplitudes.
($\dot{x}_c$: container velocity, $\dot{x}_p$: particle bed velocity, $\dot{\varphi}_p$: angular velocity of particles)

3 Energy dissipation of a particle damper

The energy dissipation of the scattering and rolling bed motion mode are presented next. To judge about the particle damper's efficiency the reduced loss factor η^* [9, 20] is used. It is calculated by a scaling of the dissipated energy per radian E_{diss} with the kinetic energy of the particle system using the mass of the particle bed m_{bed}, i.e. the mass of all particles, to

$$\eta^* = \frac{E_{diss}}{E_{kin}} = \frac{E_{diss}}{\frac{1}{2} m_{bed} \dot{X}^2}. \tag{2}$$

Scattered state: For the scattered state it can be assumed that the dissipated energy by the particles is proportional to the kinetic energy of the particle system and the number of particle–wall collisions. As the particles hitting the container walls at random phases, a higher excitation amplitude leads to more collisions while a higher clearance to less. Based on an empirical approach, this results in

$$E_{diss} = \kappa \frac{X}{h} E_{kin} = \kappa \frac{X}{h} \frac{1}{2} m_{bed} \dot{X}^2, \tag{3}$$

with κ being an empirical scaling factor. For this energy dissipation, the reduced loss factor turns out to be

$$\eta^* = \kappa \frac{X}{h}. \tag{4}$$

Equation (4) is remarkable as it is only depending on the container amplitude and clearance but not on the excitation frequency. Comparisons with experiments have shown that $\kappa = 1$ is leading to the best results. As here the same particle container is used, see also Fig. 3, this value is adopted. The reduced loss factor of the scattered state is shown in Fig. 2 for $X < X_{opt}$. The reduced loss factor starts close to 0 for very low container amplitudes $X \ll X_{opt}$ and increases linearly. At the transition to the rolling bed motion

mode, i.e. at $X = X_{\mathrm{opt}}$, the highest value of 0.4 is reached.

Rolling bed: Within the rolling bed motion mode, two inelastic collisions of the particle bed with the container walls occur during one vibration cycle. Hence, the dissipated energy per cycle $\widetilde{E}_{\mathrm{diss}} = 2\pi E_{\mathrm{diss}}$ can be derived to

$$\widetilde{E}_{\mathrm{diss}} = \frac{1}{35} m_{\mathrm{bed}} \dot{X}^2 \left(\sqrt{25 + 10 \sin^2(\Omega t_{\mathrm{i}})} - 5 \cos\left(\Omega t_{\mathrm{i}}\right) \right)^2 . \tag{5}$$

In Eq. (5) only the impact time point t_{i} of the particle bed with the opposite container wall is unknown, see also Fig. 1. The impact time point is the time the particle bed travels from one container side to the other one. The impact time follows by solving numerically

$$\underbrace{\int_0^{t_{\mathrm{i}}} \dot{x}_{\mathrm{p}}(t) \mathrm{d}t}_{\text{particle motion}} = \underbrace{X \sin(\Omega t_{\mathrm{i}})}_{\text{container motion}} + \underbrace{h}_{\text{clearance}} . \tag{6}$$

In Eq. (6) only the particle velocity $\dot{x}_{\mathrm{p}}$ is unknown. It is obtained by assuming energy conservation before and after the particle bed left the pushing container wall. Using the rolling condition $\dot{\varphi}_{\mathrm{p}} = \frac{\dot{x}_{\mathrm{p}} - \dot{x}_{\mathrm{c}}}{r}$, with r being the particles' radius, ones obtains finally for the particles' velocity

$$\dot{x}_{\mathrm{p}} = \frac{1}{7} \dot{X} \left(2 \cos\left(\Omega t\right) + \sqrt{25 + 10 \sin^2\left(\Omega t\right)} \right) . \tag{7}$$

The reduced loss factor is achieved by inserting Eq. (5) into Eq. (2) and is shown in Fig. 2 for $X > X_{\mathrm{opt}}$. The reduced loss factor starts in the rolling mode with its maximum value $\eta^*_{\mathrm{max}} \approx 0.91$ and decreases to higher container amplitudes. This progression of the reduced loss factor can be explained by taking the relative velocity between particle bed and container at the impact time point into consideration. For very high container amplitudes $X \gg X_{\mathrm{opt}}$ the particle bed leaves the container wall with a high velocity. Thus, the particle bed collides almost immediately with the opposite container wall, i.e. $\Omega t_{\mathrm{i}} \to 0$. Consequently, the relative velocity at impact is comparatively low, resulting in a low efficiency. When the container amplitude decreases, the impact time point increases, and thus the relative velocity at impact. This leads to a higher efficiency. The threshold for this is at an impact time point of $\Omega t_{\mathrm{i}} = \pi$. Here, the container is again located at $x_{\mathrm{c}} = 0$ but moves in the other direction with $\dot{x}_{\mathrm{c}} = -\dot{X}$. This is the impact time point of maximum relative velocity and thus of the highest efficiency. For this time point, $X \approx 0.4h$ holds. For even lower container strokes, the system switches to the scattered state. This happens as the assumption that the particle bed leaves the pushing wall at $x_{\mathrm{c}} = 0$ is violated for the next vibration cycle otherwise.

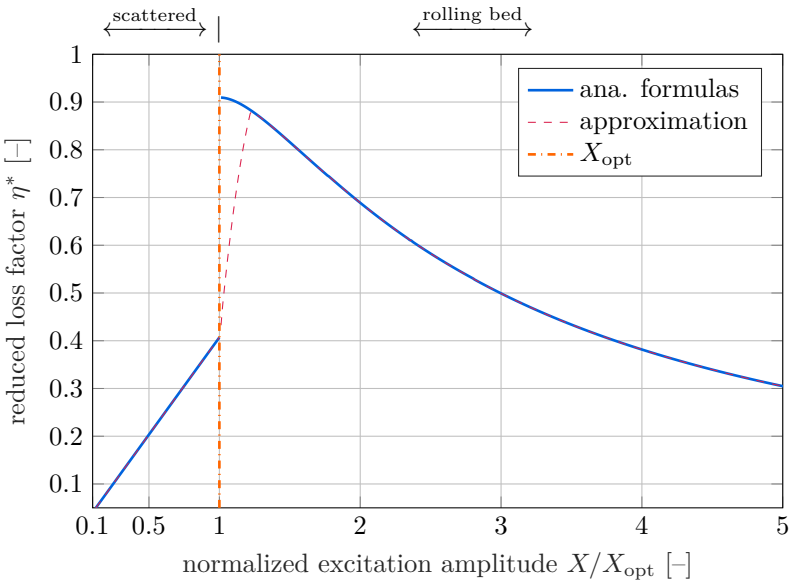

Figure 2: Reduced loss factor for scattered and rolling bed motion mode.

4 Coupling with vibrating structure

In the next step, a particle damper using the rolling attribute of spheres is utilized to damp a system with low first eigenfrequency under horizontal forced vibration. Thereby, experimental and numerical investigations are performed. The experimental obtained FRF's are compared to numerical results based on the analytical Eqs. (3) and (5) of the energy dissipation for such a particle damper. Finally, a formula for an optimal damper design is derived and validated experimentally.

4.1 Experimental setup

The experimental setup is shown in Fig. 3. It consists of a simple beam-like structure with the particle damper mounted at its tip. The elastic length of the steel beam is 512 mm with a rectangular profile of 80 mm × 2 mm and a Young's modulus of $E = 200\,\text{GPa}$. The end-effector of the beam-like structure consists of an additional mass and the particle container with a total weight of 1270 g. The particle container is made of polyvinyl chloride (PVC) and has a quadratic cross section with an inner edge width and height of 4 cm and a length L of 12 cm in excitation direction. The container's velocity is measured using a laser scanning vibrometer, the *PSV-500* from Polytec. The structure's base point is subjected to a harmonic motion of variable frequency using a linear drive. The linear drive is from SKF and Siemens, named LTSE 165. Its position is measured by the incremental encoder LIA20 of Numeric Jena with a resolution of 20 µm. The control of the linear drive is done by the motion controller Simotion D435–2 of Siemens and the Sinamics variable-speed drive with a sampling frequency of 8 kHz. For further details see [21, 22]. The measured results are saved with a sampling frequency of 1 kHz for later post-processing.

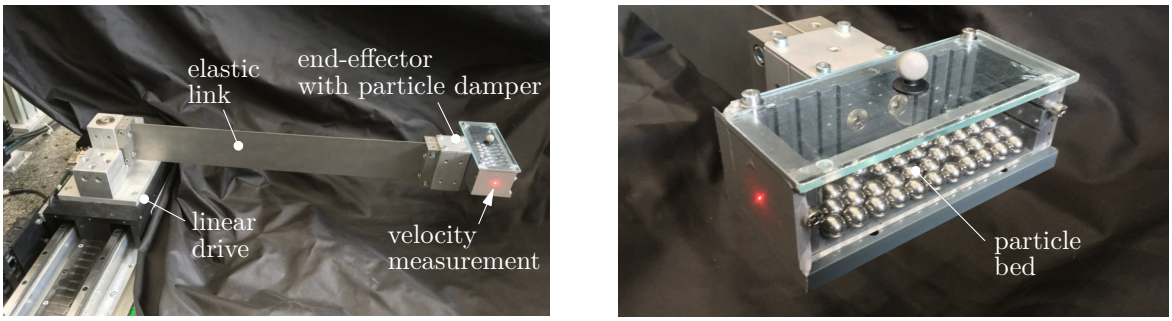

Figure 3: Overview (left) and augementation of end-effector (right) of simple beam-like structure setup.

To obtain the systems FRF, a sine sweep with linear increasing excitation frequency over time is applied to the linear drive ranging from 0.5 Hz to 4.5 Hz in 30 min. The system's FRF follows to $\boldsymbol{H}(\Omega) = \dot{\boldsymbol{X}}^*(\Omega)/\dot{\boldsymbol{U}}^*(\Omega)$ with $\dot{\boldsymbol{X}}^*$ being the fast Fourier transform (FFT) of the particle dampers velocity signal and $\dot{\boldsymbol{U}}^*$ being the FFT of the linear drives velocity signal. Each setting is measured three times and the FRF's are then combined using the complex mean [23].

4.2 Numerical model

For an efficient description of the simple beam-like structure, it is discretized with the finite element method (FEM), schematically illustrated in Fig. 4. The beam segment is made up of 100 Timoshenko beam elements. All other components are modeled as rigid bodies, due to their high stiffness and are included as point elements with their corresponding mass. The moment of inertia terms are neglected. As boundary condition a fixed frame is used, i.e. $u = 0$. To reduce the number of degrees of freedom, a modal reduction is performed. As only the first mode of the system shall be analyzed, only this one is considered for the modal reduction. Doing so leads to a system of form

$$\ddot{q} + \omega_0^2 q = \phi F, \tag{8}$$

$$x = x(y_{\mathrm{ef}}) = \phi q, \tag{9}$$

with q being the first elastic coordinate and ω_0 the angular frequency of the first mode. The shape function value in x-bending direction at the end-effector is denoted by ϕ. It projects the force F at the end-effector in x-bending direction onto the elastic coordinate. The output x is the deformation at the end-effector in x-bending direction. Inserting

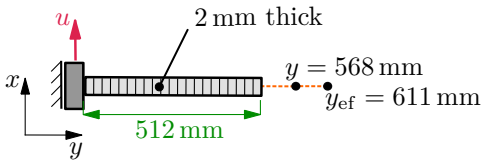

Figure 4: FEM model of the simple beam-like structure.

Eq. (9) into Eq. (8) leads to the system

$$\frac{1}{\phi^2}\ddot{x} + \frac{\omega_0^2}{\phi^2}x = F. \tag{10}$$

Rewriting this equation and introducing the structural damping coefficient of the first mode D_0, i.e. without particle damper, one obtains the typical equation of motion of a single degree of freedom system

$$M_0\ddot{x} + D_0\dot{x} + Kx = F. \tag{11}$$

The force at the end-effector F is now replaced by the particle damper force $F_{\mathrm{pd}} = -(m_{\mathrm{eff}}\ddot{x} + d_{\mathrm{eff}}\dot{x})$ and the excitation force thru the linear drive $F_{\mathrm{ld}} = UK\cos(\Omega t) - \dot{U}D_0\sin(\Omega t)$. The energy dissipation by the particle damper E_{diss} is hereby expressed as an effective viscous damping parameter d_{eff}. As the particles are temporary coupled to the container, the effective particle mass m_{eff} has to be considered as additional inertia term [24]. As the structural damping of the beam D_0 is small and for excitations near the eigenfrequency of the system $\dot{X} \gg \dot{U}$ holds, the second term of the excitation force thru the linear drive can be neglected yielding $F_{\mathrm{ld}} = UK\cos(\Omega t)$. Inserting F_{pd} and F_{ld} into Eq. (11) results finally in

$$\underbrace{(M_0 + m_{\mathrm{eff}})}_{M}\ddot{x} + \underbrace{(D_0 + d_{\mathrm{eff}})}_{D}\dot{x} + Kx = \underbrace{UK}_{R}\cos(\Omega t). \tag{12}$$

Due to the effective particle mass and the effective viscous damping parameter, Eq. (12) is a linear differential equation of second order with non-constant coefficients. Thus, to obtain the systems FRF, Eq. (12) is solved iterative for every excitation frequency successively. Hence, the frequency range is divided into 1000 sample points. To solve Eq. (12) the effective particle mass and the effective viscous damping are needed. For an excitation of constant frequency and force amplitude, the system will reach a stationary state, after its transients vanish. The particle container is then vibrating with amplitude X and the excitation frequency Ω. The effective viscous damping coefficient in a stationary state is calculated by the dissipated energy per cycle and the excitation conditions [25]. The effective viscous damping coefficient follows then to

$$d_{\mathrm{eff}} = \frac{\widetilde{E}_{\mathrm{diss}}(\Omega, X)}{\pi\Omega X^2}. \tag{13}$$

The dissipated energy per cycle $\widetilde{E}_{\mathrm{diss}}$ is obtained from Eqs. (3) and (5). However, it is hard to describe the effective particle mass analytically [24]. Here, it is assumed to be equivalent to the mass of all particles, i.e. $m_{\mathrm{eff}} = m_{\mathrm{bed}}$. However, this is an rather rough approximation.
The effective eigenfrequency ω, i.e. the undamped eigenfrequency of the system influenced by the particle mass, follows then to

$$\omega = \sqrt{\frac{K}{M}} = \sqrt{\frac{K}{M_0 + m_{\mathrm{eff}}}}. \tag{14}$$

Thus, $\omega < \omega_0$ is true. Using the analytical solution of Eq. (12), i.e. $x = X\cos(\Omega t - \psi)$, under the condition of a stationary state, the container's amplitude X and the damping ratio ζ follow to

$$\zeta = \frac{D}{2M\omega}, \tag{15}$$

$$X = \frac{R/M}{\sqrt{\left(\omega^2 - \Omega^2\right)^2 + \left(2\zeta\omega\Omega\right)^2}}. \tag{16}$$

However, Eq. (13)–Eq. (16) are depending on each other via the dissipated energy of the particle damper, causing the effective viscous damping coefficient to be non-constant. Thus, a fixed-point iteration scheme is used to solve these equations, see Fig. 5. It turns out that the jump in the reduced loss factor between scattered and rolling bed motion mode, see Fig. 2, leads to convergence problems of the fixed-point iteration scheme. Thus, a smoothing function is used to avoid this problem, see "approximation" in Fig. 2. In the performed studies, the iteration scheme converges in general in five to ten iterations.

4.3 Results

In a first step, the numerical model of the simple beam-like structure shall be validated. From the modal reduction the mass and stiffness at the end-effector, see Eq. (11), follow to $M = 1058\,\mathrm{g}$ and $K = 143\,\mathrm{N/m}$. The eigenfrequency of the undamped system is $f_0 = \omega_0/(2\pi) = 1.85\,\mathrm{Hz}$. In Fig. 6 numerical and experimental FRF's are compared for an excitation amplitude of $U = 0.25\,\mathrm{mm}$ using no particles. The numerical obtained eigenfrequency is very close to the experimental measured one with only a difference of $0.02\,\mathrm{Hz}$. The structural damping parameter D_0 is obtained from measurements and is with a value of $0.032\,\mathrm{kg/s}$ rather small. The envelope of the FRF's fit well. However, for frequencies above the eigenfrequency, the difference is slightly increasing. This is because the numerical model only considers the first eigenmode. However, in the experiments, the second eigenmode of the system is also excited, leading to an increases amplitude.
As the accuracy of the numerical model without particles has been validated, in the next step 36 spherical steel particles of $5\,\mathrm{mm}$ radius weighting $147\,\mathrm{g}$ are filled in the particle container. The resulting clearance and optimal stroke are $h = 30\,\mathrm{mm}$ and $X_{\mathrm{opt}} = 12\,\mathrm{mm}$, respectively, see Eq. (1) and Fig. 1. To check the proposed numerical calculation scheme for the FRF, see Fig. 5, numerical results are compared to experiments for two excitation amplitudes of $U = 0.5\,\mathrm{mm}$ and $U = 2\,\mathrm{mm}$. The results are presented in Fig. 7. Additionally, in both figures the FRF of the undamped system is plotted and the value of the normalized optimal stroke X_{opt}/U for the corresponding excitation amplitude is added.
From both figures, it is seen that the reduction of the systems eigenfrequency, due to the temporary coupled particle mass, is well approximated. In both cases, the eigenfrequency reduces to about $f = 1.73\,\mathrm{Hz}$. For an excitation of $U = 0.5\,\mathrm{mm}$ the simulations FRF peak agrees well with the experiment. As the peak's amplitude is below the optimal stroke, the particle bed is still in the scattered state. However, for excitation frequencies slightly above the damped eigenfrequency, somewhat bigger differences occur. While in

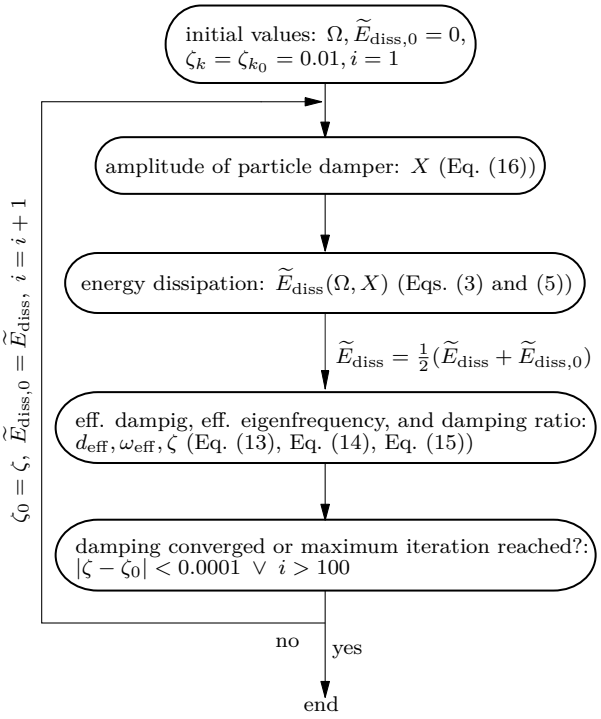

Figure 5: Fixed-point iteration scheme to find solution of Eq. (12).

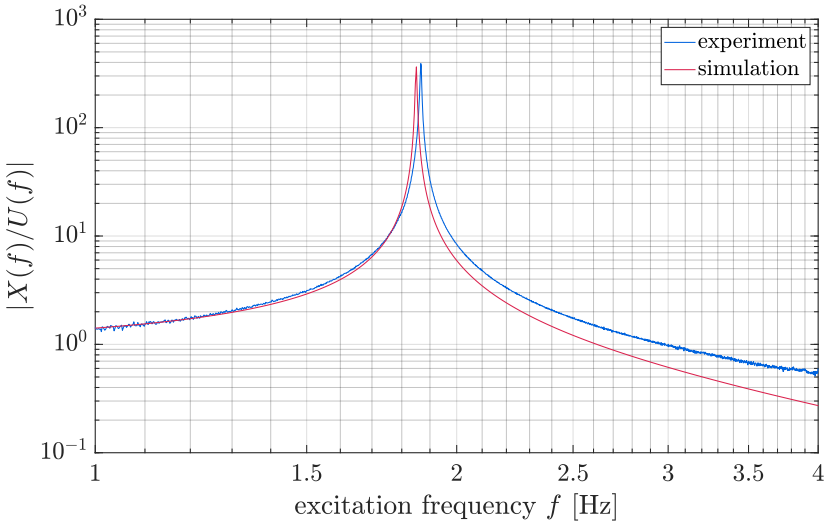

Figure 6: Comparison of numerical and experimental FRF of undamped system for $U = 0.25\,\mathrm{mm}$.

a) $U = 0.5\,\mathrm{mm}$.

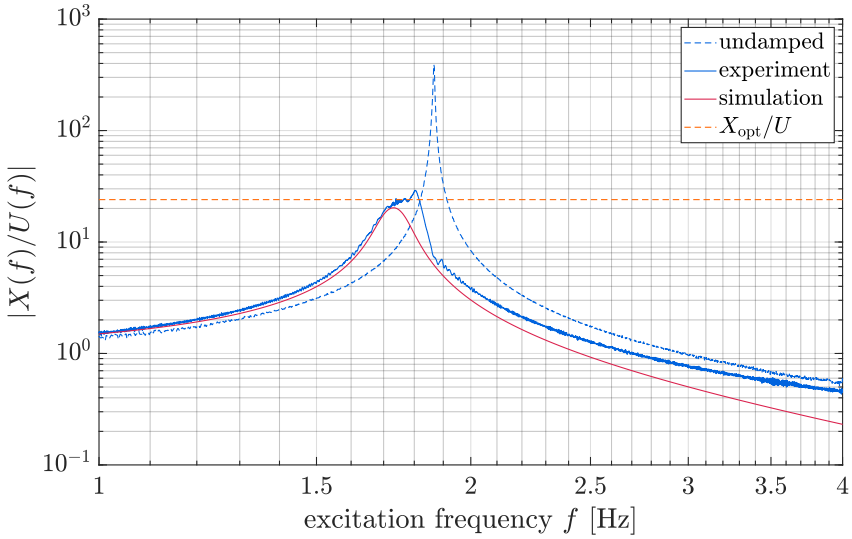

b) $U = 2\,\mathrm{mm}$.

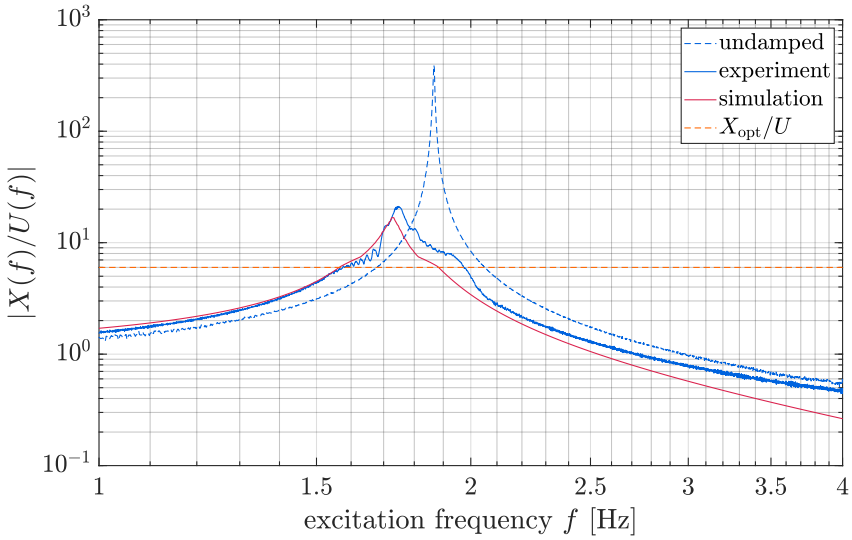

Figure 7: Comparison of numerical and experimental FRF of damped system for a) $U = 0.5\,\mathrm{mm}$ and b) $U = 2\,\mathrm{mm}$.

the simulation the amplitude is reducing as expected, in the experiment the opposite happens. The vibration amplitude even reaches the threshold X_{opt}/U. This behavior occurs since the assumption of $m_{\mathrm{eff}} = m_{\mathrm{bed}}$ is violated for vibration amplitudes of the scattered state close to X_{opt}. In this area, $m_{\mathrm{eff}} \ll m_{\mathrm{bed}}$ holds. Thus, the system's eigenfrequency is increasing, resulting in the observed behavior. The damping ratio of simulation and experiment follow at the FRF's peaks to $\zeta = 2.5\,\%$ and $\zeta = 1.7\,\%$, respectively. These values are on a similar scale and are much higher compared to the undamped case of $\zeta = 0.13\,\%$.
For an excitation of $U = 2\,\mathrm{mm}$ the simulations FRF peak agrees well with the experiment again, see Fig. 7b). The peaks of both FRF's are above the threshold amplitude X_{opt}/U, i.e. the rolling bed motion mode is seen here. In contrast to Fig. 7a), for excitation frequencies slightly above the eigenfrequency, somewhat smaller differences are obtained. The damping ratio of simulation and experiment follow at the FRF's peaks to $\zeta = 2.9\,\%$ and $\zeta = 2.4\,\%$. This might wonder since these values are only slightly higher as for the scattered state of Fig. 7a). However, the resulting container's amplitude is for $U = 2\,\mathrm{mm}$ about $X = 40\,\mathrm{mm}$ and thus way above the optimal stroke of $X_{\mathrm{opt}} = 12\,\mathrm{mm}$. For such high amplitudes, the reduced loss factor is already much reduced compared to the optimal case, see also Fig. 2.
For both conducted experiments, the experimental damping ratio deviates from the numerical results due to inaccuracies and imperfections of the experimental setup. These are amongst others, a little tilt around the container's axis, an additional rotation of the container thru the bending of the beam, a torsional movement due to the low beam torsion constant, and a non perfect rolling movement of the particles. These parameters significantly influence the particle motion and thus the energy dissipation. Still, the proposed calculation scheme, shown in Fig. 5, is suitable to obtain the system's FRF and a first good approximation of the resulting damping ratio.

Optimal damper: In Fig. 7 it is seen that it is possible to damp the simple beam-like structure as well using the scattered state as using the rolling bed motion mode of the particle bed. However, in both cases, the efficiency of the particle damper is way below its optimum. The damper's highest efficiency is reached at X_{opt}, see also Fig. 2. Hence, an operation of the particle damper with amplitude X_{opt} should be desired. In this state, the energy dissipation is obtained to

$$\widetilde{E}_{\mathrm{diss}}^{\mathrm{max}} = \frac{20}{7} m_{\mathrm{bed}} \dot{X}^2. \tag{17}$$

Inserting Eq. (17) into Eq. (13) and this one into Eq. (15) and neglecting the structural damping, one obtains the optimal damping ratio for a given particle damper, i.e. an operation at X_{opt}, to

$$\zeta_{\mathrm{opt}} = \frac{10 m_{\mathrm{bed}}}{7\pi M}. \tag{18}$$

For the utilized system the optimal damping ratio results in $\zeta_{\mathrm{opt}} = 5.5\,\%$. This damping ratio is about twice as high as those obtained from Fig. 7. Thus, the question arises of

how to design the particle damper, such that it is operated in its optimal operation point X_{opt}. To answer this, Eq. (18) is inserted in Eq. (16) and an excitation in the systems effective eigenfrequency $\Omega = \omega$ is assumed. Solving this equation for the mass of the particle bed, one obtains

$$m_{\mathrm{bed,opt}} = \frac{\pi R M_0}{\frac{20}{7} K X_{\max} - \pi R}. \tag{19}$$

The desired maximum vibration amplitude during resonance is given by $X_{\max}$. Using this desired maximum amplitude, the necessary clearance follows to $h = 2.5 X_{\max}$. One should keep in mind that these equations are only valid as long $\ddot{X}_{\max} < g$ holds as otherwise the rolling condition of the spherical particles is violated.
To validate Eq. (19) it is applied to the simple beam-like structure. However, as the particle container is already manufactured, Eq. (19) is rewritten such that the necessary excitation amplitude U_{opt} is obtained to excite the given particle container in its optimal state. For this, one achieves

$$U_{\mathrm{opt}} = \frac{20 m_{\mathrm{bed}} \omega^2}{7 \pi K} X_{\mathrm{opt}}. \tag{20}$$

Note, a direct correlation between Eqs. (19) and (20) is hard to see as the system's effective eigenfrequency ω depends on the particle bed mass m_{bed}, see Eq. (14). As the particle bed mass is known in Eq. (20) this term is rather simple. However, Eq. (19) is solved for the particle bed mass, resulting in a more complex expression.
Applying Eq. (20) to the simple beam-like structure using 36 particles, results in $U = 1.34\,\mathrm{mm}$. The corresponding FRF's of simulation and experiment are shown in Fig. 8. The FRF's envelope of simulation and experiment fits well. However, during resonance little higher amplitudes in the experiments are seen. Also, for excitation frequencies slightly above the eigenfrequency, almost no reduction in the vibration amplitude is observed. This happens due to the high sensitivity of the dissipation energy and effective particle mass around the optimal stroke, see Fig. 2. The damping ratios of simulation and experiment result in $\zeta = 4.8\,\%$ and $\zeta = 3.7\,\%$, respectively. These values are quite lower than the optimal damping ratio $\zeta_{\mathrm{opt}} = 5.5\,\%$ but much higher as the damping ratios obtained from Fig. 7 with values between $\zeta = 1.7 - 2.9\,\%$.
Theoretically, in the optimal case during resonance, a container amplitude of $X = X_{\mathrm{opt}}$ is achieved and thus an energy dissipation of $\tilde{E}_{\mathrm{diss}}^{\max}$ occurs. However, in Fig. 8 it is seen that the simulation result crosses the X_{opt}/U threshold instead of touching it. This happens due to the approximation made for the dissipated energy between scattered and rolling bed motion mode, see Fig. 2. Thus, the theoretical value for the maximum dissipated energy is not reached in the simulation. This also explains the difference between the optimal damping ratio and damping ratio obtained from simulation.
Due to inaccuracies occurring during the experiment, like a tilt of the container, the experimental damping ratio is lower as the numerical result. Reducing the effect of these influence parameters might significantly increase the measured damping and thus reduce

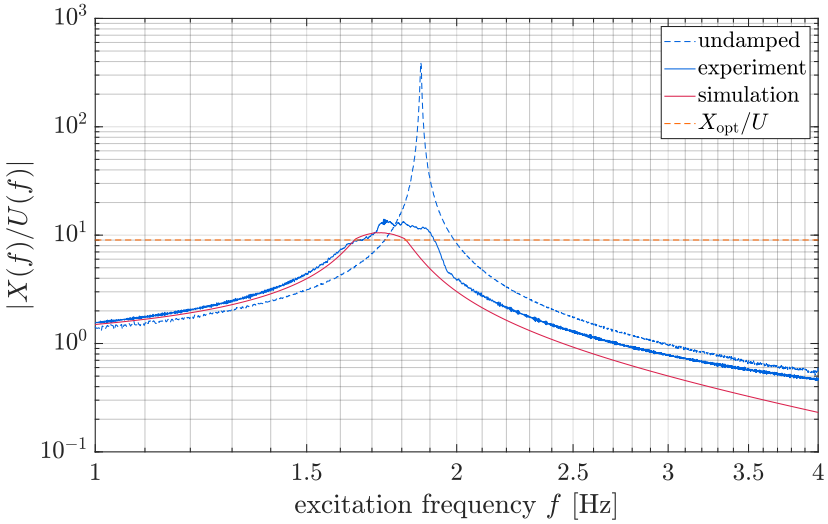

Figure 8: Comparison of numerical and experimental FRF of simple beam-like structure under theoretical optimal excitation of $U = 1.34\,\text{mm}$.

the difference between simulation and experiment. With the utilized system this is indeed not possible. Still, Eq. (19) enables a simple, accurate, and quick design of particle dampers for horizontal, forced vibrations of low acceleration amplitudes. However, special care on precise manufacturing, mounting, and operation are necessary.

5 Conclusion

Subjecting a container with a flat base filled with spherical particles to a horizontal sinusoidally motion, two different motion modes of the particle bed can be observed for container accelerations below the gravitational acceleration. These two motion modes, called scattered and rolling bed, can be used to damp structures under horizontal forced vibration. The design approach to do so, is presented here.

In a first step, the energy dissipation progression inside a horizontally driven particle damper is presented, i.e. without underlying structure. For low container vibration amplitudes, the particle system is in the scattered state. Here, no synchronous motion of the particle system is seen, resulting in a comparatively low energy dissipation and efficiency. Increasing the container vibration amplitude above a certain threshold amplitude, the particle system switches to the rolling bed motion mode. Within the rolling bed, particles form one particle block and collide inelastically with the container walls. Thus, a high energy dissipation and efficiency can be obtained. However, for increasing vibration amplitudes the efficiency of the damper is decreasing slightly. It turns out that the energy dissipation of both motion modes can be described accurately using analytical formulas, although the particle movement is highly non-linear.

In the second step, experimental studies on a simple beam-like structure are performed. The base point of the beam is subjected to a harmonic motion of variable frequency using a linear drive. The particle damper is mounted at the tip of the beam filled with spherical steel particles and its velocity is measured using a laser scanning vibrometer. Thus, the

frequency response function is obtained. Also, a numerical model of the system is set up. The model is coupled to the analytical formulas describing the energy dissipation of the particle bed by using an equivalent viscous damping parameter. A good agreement between simulations and experiments is achieved, while operating the particle damper as well in its scattered state as in its rolling bed state.
Finally, the coupled model is used to calculate the design parameter of the particle damper to operate it at its maximum efficiency. A simple analytical expression is obtained. Its accuracy is proven numerically. However, due to inaccuracies within the experiment setup, some differences remain here. Still, the formula provides a powerful tool to design particle damper for applications of low acceleration intensity.

Acknowledgments

The authors would like to thank the German Research Foundation (DFG) for the financial support of the project SE1685–8/1. The authors would also like to thank Dr.-Ing. Marc-André Pick, Dipl.-Ing. Riza Demir, Dipl.-Ing. Norbert Borngräber-Sander and Wolfgang Brennecke for helping to design and realize the experimental rig.

References

[1] C. D. Johnson, Design of passive damping systems, Journal of Mechanical Design 117 (B) (1995) 171–176. doi:10.1115/1.2838659.

[2] T. Chen, K. Mao, X. Huang, M. Wang, Dissipation mechanisms of nonobstructive particle damping using discrete element method, Proceedings of SPIE - The International Society for Optical Engineering 4331 (2001) 294–301. doi:10.1117/12.432713.

[3] H. Panossian, Non-obstructive particle damping experience and capabilities, Proceedings of SPIE - The International Society for Optical Engineering 4753 (2002) 936–941. doi:10.2514/6.2008-2102.

[4] S. S. Simonian, Particle beam damper, Proceedings of SPIE - The International Society for Optical Engineering 2445 (1995) 149–160. doi:10.1117/12.208884.

[5] H. Panossian, Structural damping enhancement via non-obstructive particle damping technique, Journal of Vibration and Acoustics 105 (114) (1992) 101–105. doi:10.1115/1.2930221.

[6] I. H. Ansari, M. Alam, Patterns and velocity field in vertically vibrated granular materials, AIP Conference Proceedings 1542 (1) (2013) 775–778. doi:10.1063/1.4812046.

[7] Y. Duan, Q. Chen, Simulation and experimental investigation on dissipative properties of particle dampers, Journal of Vibration and Control 17 (5) (2010) 777–788. doi:10.1177/1077546309356183.

[8] P. Eshuis, K. Weele, D. Meer, D. Lohse, Granular leidenfrost effect: Experiment and theory of floating particle clusters, Physical review letters 95 (2006) 258001. doi:10.1103/PhysRevLett.95.258001.

[9] M. Masmoudi, S. Job, M. S. Abbes, I. Tawfiq, M. Haddar, Experimental and numerical investigations of dissipation mechanisms in particle dampers, Granular Matter 18 (3) (2016) 71. doi:10.1007/s10035-016-0667-4.

[10] A. J. Matchett, T. Yanagida, Y. Okudaira, S. Kobayashi, Vibrating powder beds: A comparison of experimental and distinct element method simulated data, Powder Technology 107 (1) (2000) 13–30. doi:10.1016/S0032-5910(99)00080-7.

[11] C. Saluena, S. E. Esipov, T. Poeschel, S. S. Simonian, Dissipative properties of granular ensembles, Proceedings of SPIE 3327 (1) (1998) 23–29. doi:10.1117/12.310696.

[12] C. X. Wong, M. C. Daniel, J. A. Rongong, Energy dissipation prediction of particle dampers, Journal of Sound and Vibration 319 (1-2) (2009) 91–118. doi:10.1016/j.jsv.2008.06.027.

[13] Z. Yin, F. Su, H. Zhang, Investigation of the energy dissipation of different rheology behaviors in a non-obstructive particle damper, Powder Technology 321 (2017). doi:10.1016/j.powtec.2017.07.090.

[14] K. Zhang, T. Chen, L. He, Damping behaviors of granular particles in a vertically vibrated closed container, Powder Technology 321 (2017) 173–179. doi:10.1016/j.powtec.2017.08.020.

[15] Z. Lu, D. Wang, S. Masri, X. Lu, An experimental study of vibration control of wind-excited high-rise buildings using particle tuned mass dampers, Smart Structures and Systems 18 (2016) 93–115. doi:10.12989/sss.2016.18.1.093.

[16] K. Zhang, T. Chen, X. Wang, J. Fang, Rheology behavior and optimal damping effect of granular particles in a non-obstructive particle damper, Journal of Sound and Vibration 364 (2015). doi:10.1016/j.jsv.2015.11.006.

[17] A. Sack, M. Heckel, J. Kollmer, F. Zimber, T. Pöschel, Energy dissipation in driven granular matter in the absence of gravity, Physical review letters 111 (2013). doi:10.1103/PhysRevLett.111.018001.

[18] M. Sanchez, G. Rosenthal, L. Pugnaloni, Universal response of optimal granular damping devices, Journal of Sound and Vibration 331 (20) (2012) 4389–4394. doi:10.1016/j.jsv.2012.05.001.

[19] M. N. Bannerman, J. E. Kollmer, A. Sack, M. Heckel, P. Mueller, T. Pöschel, Movers and shakers: Granular damping in microgravity, Physical Review E 84 (2011). doi:10.1103/PhysRevE.84.011301.

[20] N. Meyer, R. Seifried, Toward a design methodology for particle dampers by analyzing their energy dissipation, Computational Particle Mechanics (2020). doi:10.1007/s40571-020-00363-0.

[21] M. Morlock, N. Meyer, M.-A. Pick, R. Seifried, Modeling and trajectory tracking control of a new parallel flexible link robot, in: Proceedings of the 2018 IEEE/RSJ International Conference on Intelligent Robots and Systems, 2018. doi:10.1109/IROS.2018.8594008.

[22] M. Morlock, N. Meyer, M.-A. Pick, R. Seifried, Real-time trajectory tracking control of a parallel robot with flexible links, Mechanism and machine theory 158 (2021) 104220. doi:10.1016/j.mechmachtheory.2020.104220.

[23] A. Brandt, Noise and Vibration Analysis: Signal Analysis and Experimental Procedures, John Wiley and Sons, Ltd, Chichester, UK, 2011. doi:10.1002/9780470978160.

[24] M. Sanchez, L. Pugnaloni, Effective mass overshoot in single degree of freedom mechanical systems with a particle damper, Journal of Sound and Vibration 330 (2011). doi:10.1016/j.jsv.2011.07.016.

[25] A. A. Shabana, Theory of Vibration: An Introduction, 3rd Edition, Springer, Cham, 2019. doi:10.1007/978-1-4612-3976-5.